Photoconductor Charging Modeling For Color Laser Printing System

Joong-Gwang Shin, Junhee Cho, Inyong Song, and Kyucheol Shin
Samsung Electronics Co., LTD.
Suwon, Korea

Abstract

The plural charging devices are necessary to charge a photoconductor for a latent image formation in color laser printing systems. In this research, characteristics of the charging device for a liquid toner based color printing system have been investigated. To develop a mathematical model for the photoconductor charging characteristics, the charging current to the photoconductor can be determined by experimental investigations. The experimental set-up consists of the primary charging part and the secondary charging part, and this carries out to investigate the charging characteristics of the device. Once the mathematical model is developed, the parametric design of the charging device for the proposed system can be conducted through simulation runs and compared with experiments. The complete design is adapted and performed with Samsung's color printing system.

Introduction

To produce a latent image on the photoconductor, it is necessary to charge the surface of the photoconductor. A corotron device discussed in [1] through [3] is a typical charging method in electrophotographic system and plural corotron devices are used to recharge the photoconductor after developing process for the next following latent image formation in color printing system. In this research, the initial charging process is referred to a primary charging process, and the recharging process is referred to a secondary charging process.

A uniform charge distribution on the photoconductor is generated by absorbing ionized molecules that occurs from an electrical corotron device employing thin wires with very high potentials. The surface potential of the photoconductor is dependent upon wire current, grid voltage, and gap between the photoconductor and the charging device, and it can be calculated by measuring the charging current to the photoconductor. In the proposed research, the primary and the secondary charging devices are designed and performed by understanding the relationship between the charging current and the surface potential characteristics of the photoconductor and by choosing the appropriate system parameter values for Samsung's color printing system.

Configuration of Charging Device

The efficiency of charging device is determined by its geometry, number of corona wires, and distance from wire to photoconductor, and it is referred to [4] and [5]. In general, color laser printing system requires a number of charging devices dependent upon system configurations. In this proposed system, a primary charger and 4 of secondary chargers are used, and the polarity of the chargers is set to be positive. The function of the primary charger adapting the scorotron charging method is to charge an appropriate potential on the photoconductor initially. The charging potential by the primary charger is usually within the range of 600V-800V. The function of the secondary chargers adapting the corotron charging method is to restore proper charging potential on the photoconductor after developing images for the next following latent image formation, and this process remains the charging potential on the photoconductor as the initial charged potential level. The configuration for the primary and secondary charging devices are shown in Fig. 1.

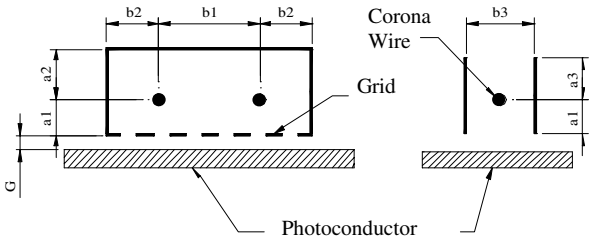

Primary charger Secondary charger

Figure 1. A Schematic Diagram of Charging Device

As shown in Fig. 1, the charging unit is held stationary with maintaining a certain gap, *G*, between the photoconductor and the charging unit. Two wires for the primary charger are positioned in parallel within the shield, and one wire for the secondary is located at the center of the shield. The gap between the photoconductor and the charging unit, the dimensions of the charging unit, and the

placing locations of the wires are the design parameters, and the charging efficiency is affected by these parameters.

Charging Potential

The general form of the charging potentials is given by

$$q(x) = cV(x), \quad (1)$$

where $q(x)$ is charge per unit area on photoconductor, c is the capacitance of the photoconductor, and x explains the displacement in the direction of the process. Taking the time derivative for both sides in Eqn.(1), the charge density, $J(x)$, may be written by

$$J(x) = cv\frac{dV}{dx}, \quad (2)$$

where v is the velocity of the photoconductor. The charge density shown in Eqn.(1) can also be explained as a function of the charging current, *I(V)*, and the charge density distribution, $G(x)$, and this relationship can be written as

$$J(x) = I(V)G(x). \quad (3)$$

Typically, the charging current per unit length, *I(V)*, may be obtained through experiments, and the charge density distribution, $G(x)$, is assumed to be Gaussian. Therefore, the charge density distribution for the primary charger, $G(x)$, may be given by

$$G(x) = B\left\{\exp\left(-A^2\left(\frac{x-b_1}{2}\right)^2\right)+\exp\left(-A^2\left(\frac{x+b_1}{2}\right)^2\right)\right\}, \quad (4)$$

where b_1 is the distance between corona wires as shown in Fig.1, and *A* and *B* are constants. For the secondary charger, one charge density distribution can be developed, therefore, the second term within Eqn.(4) can be canceled out and the dimension between the wires can be neglected.

Substituting Eqn.(3) into Eqn.(2) and taking integrals with respect to reference values of the potential and the displacement, a following relationship can be obtained.

$$\int_{V_i}^{V}\frac{dV}{I(V)} = \int_{x_i}^{x}\frac{G(x)}{cv}dx. \quad (5)$$

Since the function, $G(x)$, is normally distributed, the integration of Gaussian shown in Eqn.(4) can be described by error function, and the result of this error function may be given by

$$\int_{x_i}^{x} G(x)\,dx = \frac{1}{4}\left\{erf\,(A(x-\frac{b_1}{2}))+erf\,(A(x+\frac{b_1}{2}))\right\}$$

$$-\frac{1}{4}\left\{erf\,(A(x_i-\frac{b_1}{2}))+erf\,(A(x_i+\frac{b_1}{2}))\right\}. \quad (6)$$

Therefore, Eqn.(5) can be rewritten as

$$\int_{V_i}^{V}\frac{cvdV}{I(V)} = \frac{1}{4}\left\{erf\,(A(x-\frac{b_1}{2}))+erf\,(A(x+\frac{b_1}{2}))\right\}$$

$$-\frac{1}{4}\left\{erf\,(A(x_i-\frac{b_1}{2}))+erf\,(A(x_i+\frac{b_1}{2}))\right\} \quad (7)$$

To complete solving Eqn.(7), the parameters, *I(V)*, A, B, and b_1, should be determined. The result shown in Eqn.(7) is referred as the charging potential model for the primary charger, and it can be extended for the secondary charger. As mentioned earlier, the charging current, *I(V)*, can be determined from experiments with the process speed, v=8.13 $cm/\sec.$, and the capacitance of the photoconductor, c=290 pF/cm^2, and the others are the dimensional parameters of the charging devices shown in Fig. 1.

Experiments

To investigate the characteristics of the surface charging potential of the photoconductor, it is necessary to understand the behavior of the corona current for the proposed charging devices and the corona current can be measured experimentally over the ranges of the corona voltage and the plate potential. Fig. 2 shows a schematic of the experiment to investigate variation effects of the corona current to the plate with changing the wire current, the grid voltage, and the gap between the grid and the plate.

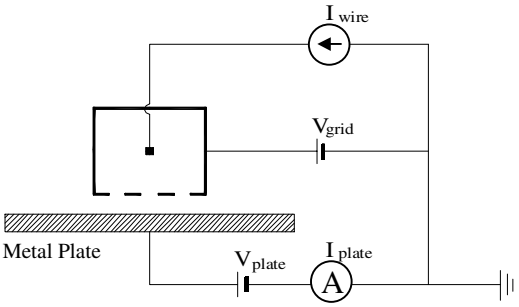

Figure 2. Experimental Set-Up

As shown in Fig. 2, the voltage devices produce very high voltage to the wire, the grid, and the plate independently. Then, the current and voltage through the wire, the grid, and the plate are monitored and controlled by a computer.

In the experiment, the corona wire current is produced from a high-voltage supply unit with changing the input current, *Iw*, from 80 μA to 500 μA. The current to the plate is measured simultaneously as a function of the plate potential from $0V$ to $800V$. This current to the plate is also carried out and monitored with changing of the grid potential. The gap between the photoconductor and the charging devices may be initially set to proper reference

values, and the variation effects of the gap should be experienced.

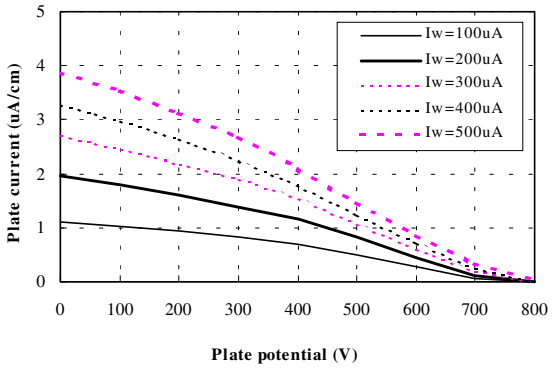

Figure 3. Plate current vs. plate potential for primary charging device

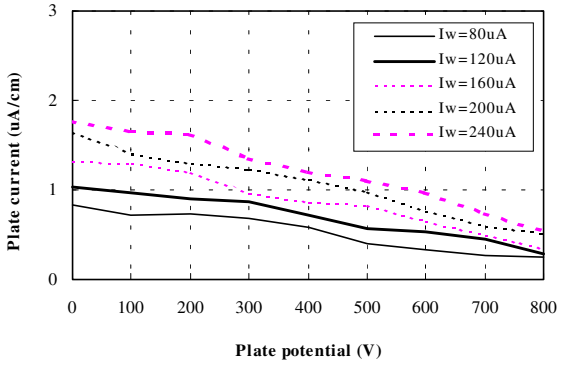

Figure 4. Plate current vs. plate potential for secondary charging device

Fig. 3 and Fig. 4 show the variation effects of the corona current to the plate per unit length of the wire with the changing the wire current, the grid voltage, and the plate potential. The magnitude of the corona current to the plate is proportionally increased when the wire current is increased. It is also shown that the corona current flowing to the plate is decreased linearly as the plate potential is increased. This means the corona current to the photoconductor is decreased as the charged surface potential of the photoconductor is increased. From Fig. 3 and 4, the experiments for the characteristics of the primary and secondary charger are carried out with three different grid potentials, 700*V*, 800*V*, and 900*V*. When the grid potentials are set to 800*V* and 900*V*, the results show the similar pattern of Fig. 3 with the change of the current magnitude only. It should also be noticed that the current magnitude is increased as the grid potential is increased. In general, the screen grid is added between the corona wire and the photoconductor to produce more uniform photoconductor charging, and the approximate maximum photoconductor potential is determined by the grid potential. The analysis related to the effect of scorotron is shown in (4) and (5). Fig. 3 and 4 shows the comparable grid effects of the corona current between the primary charger and the secondary charger.

Based on the results shown in above, the current to the plate is considered as the charging current to the photoconductor mentioned in Eqn.(3), and it may be approximated for analytic results or substituted into Eqn.(7) for numerical results.

Model Development

Based upon the experiments, the charging current, *I(V)*, for the primary and the secondary charging devices can be approximated with the curve-fit of Fig. 3 and Fig. 4, and they may be given by

$$I_P(V) = -c_1 V + c_2 , \tag{8}$$

$$I_S(V) = -c_3 V + c_4 . \tag{9}$$

where I_P and I_S represent the charging currents for the primary and the secondary respectively, and the constant, c_1, c_2, c_3 and c_4, can be approximated and selected from the experimental results shown in Fig.3 and Fig.4.

Considering the geometrical shape of the primary charging device shown in Fig. 1, the constants, *A* and *B*, shown in Eqn.(4) can be found to be $A = 1.7308 / b_2$ and $B = A/2\sqrt{\pi}$ for the primary charger. Substituting these constants values with Eqn.(8) into Eqn.(7) and rearranging them altogether, the charging potential for the primary charger may be given by

$$V_p(x) = \frac{c_2}{c_1}\left\{1 - \exp\left(-\frac{c_1\alpha_1}{cv}\right)\right\} + V_i \exp\left(-\frac{c_1\alpha_1}{cv}\right), \tag{10}$$

where α_1 is the integration of Gaussian shown in Eqn.(6). and Eqn.(10) may be solvable numerically by choosing appropriate parameter values dependent upon the design consideration. The leakage current is considered as 5% of the maximum charging current for this type of the primary charger unit to determine the constant, *A*, within Eqn.(10)

The numerical results of Eqn.(10) shown in Fig. 5 are generated with different initial surface potentials of the photoconductor, and it should also be emphasized that the results are obtained with one particular set of the charging current conditions shown in Fig. 3. Different conditions of the charging current and the grid voltage can be selected to calculate the final charging potential of the photoconductor for the desired design parameters. In reality, the instantaneous surface potential of the photoconductor as it is entered to the beginning point of the charging device may not be 0V because of the residual surface potential of the photoconductor. Therefore, three different initial potentials are used for the practice purpose.

As shown in Fig. 5, the characteristics of the charging potential of the photoconductor between three different initial potential conditions have the similar pattern. Furthermore, the experimental result is well matched with the numerical simulation runs.

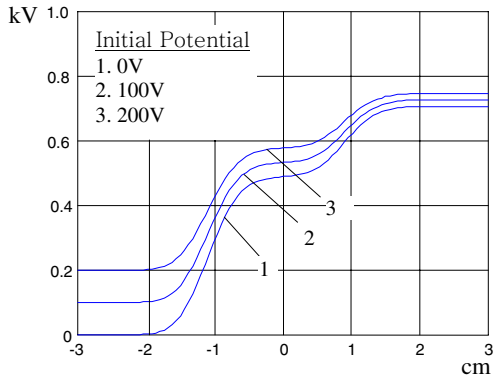

Figure 5. Calculated charging potential for primary charging device

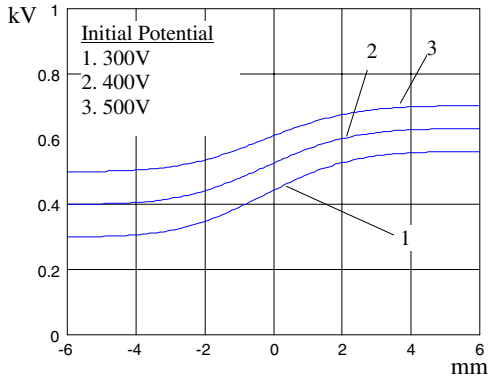

Figure 6. Calculated charging potential for secondary charging device

With the same design procedures of the primary charging device, the characteristics of the secondary charging device may be discussed. Since the leakage current for the secondary charger is considered as 1% of the maximum charging current and the constants, $A = 2.1460/(b_3/2)$ and $B = A/\sqrt{\pi}$, based on the configuration shown in Fig. 1 are determined, the charging potential for the secondary charger may be given by

$$V_p(x) = \frac{c_4}{c_3}\left\{1 - \exp\left(-\frac{c_3\,\alpha_1}{cv}\right)\right\} + V_i \exp\left(-\frac{c_3\,\alpha_1}{cv}\right), \quad (11)$$

where α_1 is the integration of Gaussian shown in Eqn.(6).

The results of the final charging potential of the photoconductor for the secondary charger are shown in Fig. 6, and compared with the experimental result. It should be also noticed that the results shown in Fig.6 are for one particular set of charging current condition shown in Fig. 4.

As mentioned in previous, the main purpose of the secondary charger for the proposed system is to recharge the photoconductor surface at a certain charging potential for the next following latent image formation. This initial surface charging potential is varied dependent upon the developing bias and the toner layer developed on the surface of the photoconductor. Therefore, the initial surface potentials on the photoconductor are set to non-zero potentials in practice. Several levels of the initial surface potential for the secondary charger are examined using Eqn.(11), and the results show that no much difference is found compared with the results shown in the primary charger.

As shown in Fig. 5 and Fig. 6, it should be noticed that the results are obtained without considering any change of the geometrical shape of the charging device. Since the charging potentials shown in Eqn.(10) and Eqn.(11) are the function of the geometrical shape of the charging device also, it may be understood that the results described in Fig. 5 and Fig. 6 should be different with changing the geometrical shape of the charging device. Based on the analytical and the experimental results, it is found that the results with changing the geometrical shape of the charging device have the similar pattern of the results shown in Fig. 5 and Fig. 6 with the slight change of the magnitude of the charging potential. Through the simulation and the experiment, the design parameters for the proposed system are found as follows: *Mechanical dimension, a_1=6, a_2=9, a_3=7.4, b_1=9, b_2=18, and b_3=12mm; wire diameter, 60um; gap between grid and photoconductor, 2-3mm.*

The details of the variation effects of the geometrical shape of the charging device are not discussed further in this paper because of the limitation of the space.

Conclusion

The analytic model for the surface charging potential on the photoconductor is investigated with the charging current flow function and the charge density distribution. The current flow function is determined experimentally, and the charge density distribution is assumed to be Gaussian. The design parameters for the charging devises affect to the surface charging potential, and these parameters are selected based upon the investigation of their variation effects. The model is performed through the experiments with the various levels of the design parameters. In particular, the result can be useful to understand the charging characteristic of the photoconductor with the variation of the process speed. For further research, the current flow function may be described as a closed-form, and it would result in the completion of the model development for the surface charging potential on the photoconductor.

Reference

1. R. G. Vyverberg, Xerography and Related Process, ed. *Focal, New York*, 1965.
2. A. J. Rushing, *IEEE Trans. AC-25, pg.1078*, 1980.
3. J. D. Cobine, Gaseous conductor, *Dover, New York,* 1958.
4. R. M. Schaffert, Electrophotography-Part II, *Focal, London*, 1980
5. L. B. Schein, Electrophotography and Development Physics, *Laplacian Press*, 1992.

Biography

Joong-Gwang Shin received his MS in Physics from the University of Inha, Korea, in 1993. He has been developed the mono-component laser beam printer at Samsung Electronics. He has been involved in process development of color laser beam printing system using liquid toners since 1997, and his work is focused on liquid development process.

Junhee Cho received his Ph.D. degree in Mechanical Engineering from the University of Missouri – Columbia, 2000 majoring mechanical dynamic system analysis. He has been involved in process development of color laser beam printing system using liquid toners at Samsung Electronics since 2000, and his work is focused on developing system analysis. He is also an active member of ASME.